NONLINEAR PHONONICS

Photo-induced chirality in a nonchiral crystal

Z. Zeng[1,2], M. Först[1], M. Fechner[1], M. Buzzi[1], E. B. Amuah[1], C. Putzke[1], P. J. W. Moll[1], D. Prabhakaran[2], P. G. Radaelli[2], A. Cavalleri[1,2]*

Chirality, a pervasive form of symmetry, is intimately connected to the physical properties of solids, as well as the chemical and biological activity of molecular systems. However, inducing chirality in a nonchiral material is challenging because this requires that all mirrors and all roto-inversions be simultaneously broken. Here, we show that chirality of either handedness can be induced in the nonchiral piezoelectric material boron phosphate (BPO_4) by irradiation with terahertz pulses. Resonant excitation of either one of two orthogonal, degenerate vibrational modes determines the sign of the induced chiral order parameter. The optical activity of the photo-induced phases is comparable to the static value of prototypical chiral α-quartz. Our findings offer new prospects for the control of out-of-equilibrium quantum phenomena in complex materials.

An object is defined as chiral if its mirror image cannot be superimposed onto itself through any combination of rotations or translations. In crystalline systems, the structural chirality is predetermined by the lattice structure during the formation process (*1*), making it challenging to manipulate the handedness of the system after growth. For example, the chiral crystal α-quartz (*2*) can exist in either right- or left-handed structures (space group $P3_121$ and $P3_221$, respectively), characterized by atomic spirals of opposite handedness within the unit cell (Fig. 1A). Once formed, chiral crystals of opposite handedness cannot be switched into each other without melting and recrystallization of the material (*3*, *4*).

Antiferrochirals are a distinct class of achiral systems in which the unit cell comprises chiral fragments with opposite handedness (*5*). The overall system remains achiral due to the degeneracy between the left- and right-handed structures, resembling racemic crystals (*6*). One notable feature of these systems is their potential to develop chirality under external perturbations that can uncompensate the staggered chiral fragments.

Inducing chirality in achiral systems by nonlinear phononics

Boron phosphate (BPO_4, space group $I\bar{4}$) is an example of an antiferrochiral material. Its equilibrium lattice and the left- and right-handed chiral substructures are sketched in Fig. 1B (*7*). The displacement of the atomic structure along the coordinates of B-symmetry modes (with amplitude Q_B) lifts the degeneracy between the local structures of opposite handedness, resulting in a ferrichiral state. Figure 2A highlights this behavior, where the shaded atomic motions along the B-mode coordinates enhance and reduce the amplitudes of the left- and right-handed local chiral structures, respectively. As a result, the handedness of the ferrichiral state can be controlled by the direction of the phonon displacement (*8*), i.e., the sign of its amplitude Q_B, providing an opportunity to rationally design the chirality in these systems by structural engineering.

This effect is not easily stimulated with external fields because it is necessary to couple to a specific lattice mode that needs to be displaced in a specific direction. This is achieved transiently through nonlinear phononics (*9*–*17*), an effective approach to coherently control the atomic structure with light. This concept provides a new basis for the rational design of crystal structures and symmetries with light, inducing desirable functional properties at high speed. In one specific type of nonlinear phononic interaction, the square of a selectively driven, infrared-active terahertz-frequency phonon mode, Q_{IR}, couples linearly to a second mode, Q_2, inducing a rectified, displacive force along the normal mode coordinate Q_2. This rectified force induces a transient crystal structure not accessible at equilibrium (*18*–*22*).

In BPO_4, a displacive force on the B-symmetry phonon modes that control chirality can be achieved by driving either of the degenerate infrared-active E-symmetry phonon modes, polarized along the *a* and *b* axes, respectively. According to the lowest-order coupling term

[1]Max Planck Institute for the Structure and Dynamics of Matter, Hamburg, Germany. [2]Department of Physics, Clarendon Laboratory, University of Oxford, Oxford, UK.
*Corresponding author. Email: andrea.cavalleri@mpsd.mpg.de

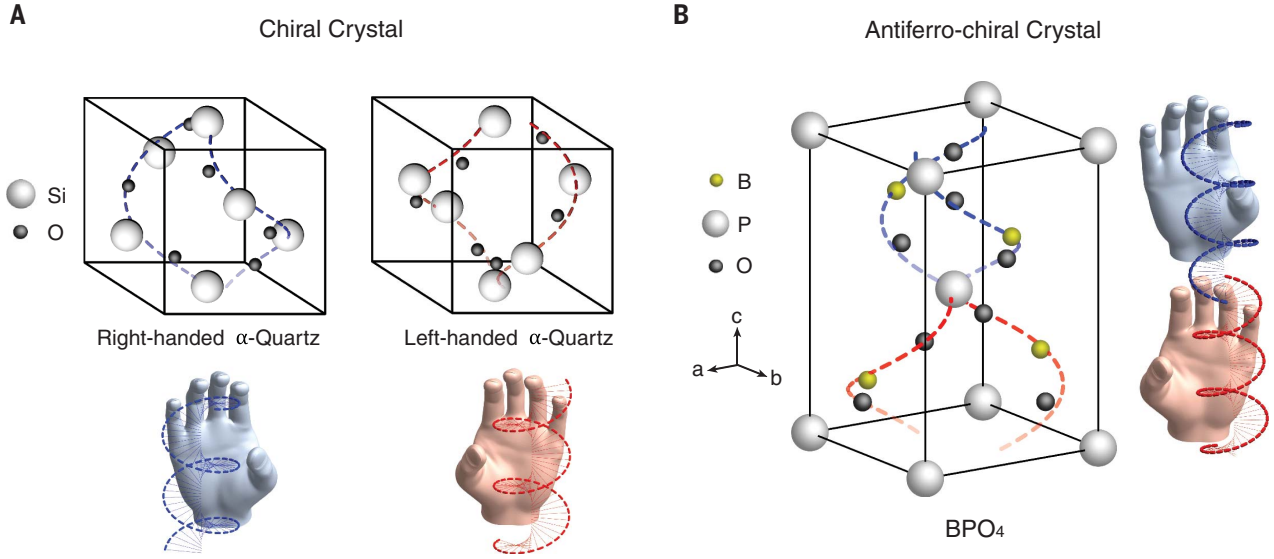

Fig. 1. Chirality in the solid state. (**A**) The prototypical chiral crystal α-quartz exists in left- and right-handed configurations that are determined by the spiral atomic structure formed during the growth process. (**B**) The unit cell of the antiferrochiral crystal BPO_4 is composed of chiral substructures of opposite handedness. The degeneracy of these left- and right-handed structures makes the overall system achiral.

Downloaded from https://www.science.org at Stiftung Deutsches Elektronen-Synchrotron on January 23, 2025

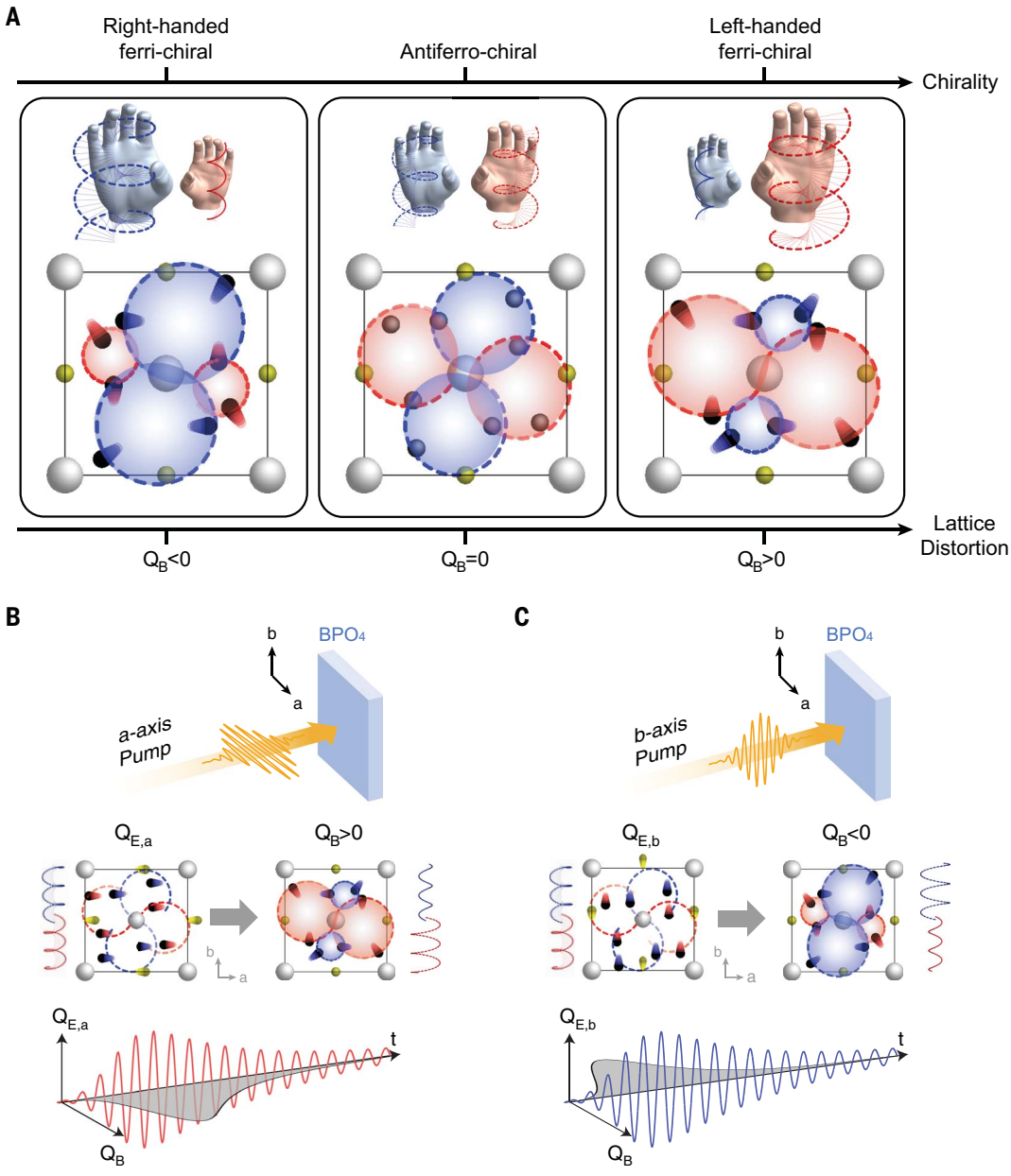

Fig. 2. Light-induced chirality in antiferrochiral BPO_4. (**A**) The atomic displacements in BPO_4 along B-symmetry phonons lift the degeneracy between the local structures of left and right handedness, driving the system from the antiferrochiral to a ferrichiral state. The phonon displacement in the opposite direction induces chirality of opposite handedness. (**B**) A terahertz pump with electric field polarization along the *a* axis induces coherent oscillations of the mode $Q_{E,a}$ about its equilibrium position. A positive transient displacement along the B-mode coordinates is induced through nonlinear phonon coupling, driving the system into the nonequilibrium ferrichiral state with left handedness. (**C**) Exciting the doubly degenerate E-symmetry phonon along the *b* axis induces coherent oscillations of the $Q_{E,b}$ mode about its equilibrium position. A negative transient displacement along the Q_B mode coordinates is induced through nonlinear phonon coupling, driving the system into a ferrichiral state with right handedness.

of the form $U = -\alpha Q_{E,a}^2 Q_B + \alpha Q_{E,b}^2 Q_B$ (*23*), the coherent drive of phonon mode $Q_{E,a}$ by a resonant terahertz-frequency field exerts a rectified force onto Q_B in the positive direction, leading to a positive transient displacement of the lattice along the B-mode coordinates away from equilibrium (Fig. 2B). Conversely, if the orthogonal mode $Q_{E,b}$ is resonantly driven, the transient displacement along Q_B changes direction due to the opposite sign in the coupling term (Fig. 2C). Therefore, the system can be driven into either one of the two opposite chiral states by controlling the polarization of the terahertz-frequency excitation pulse.

This effect can be simulated for BPO_4 through two coupled equations of motion for the resonantly driven doubly degenerate mode $Q_{E,a/b}$ and the set of four anharmonically coupled B-symmetry modes $Q_{B,i}$ (i = 1...4), taking the form

$$\frac{\partial^2}{\partial t^2} Q_{E,a/b}(t) + 2\gamma_{E,a/b} \frac{\partial}{\partial t} Q_{E,a/b}(t) + \omega_{E,a/b}^2 Q_{E,a/b}(t) = Z_{E,a/b}^* E(t) \quad (1)$$

$$\frac{\partial^2}{\partial t^2} Q_{B,i}(t) + 2\gamma_{B,i} \frac{\partial}{\partial t} Q_{B,i}(t) + \omega_{B,i}^2 Q_{B,i}(t) = \pm\alpha Q_{E,a/b}^2 \quad (2)$$

Where $\gamma_{E,a/b}$ and $\gamma_{B,i}$ are the damping coefficients, $\omega_{E,a/b}$ and $\omega_{B,i}$ the frequencies of the phonon modes, and $Z_{E,a/b}^*$ is the effective charge that couples the infrared-active $Q_{E,a/b}$ modes to the pulsed terahertz electric field $E(t) = E_0 \sin(\omega_{B,i} t) e^{-\frac{t^2}{2\sigma^2}}$. The sign of the force on the B-symmetry modes (right side of Eq. 2) depends on whether the E-symmetry mode is excited along the *a* or the *b* axis. We used ab initio calculations to determine all the relevant phonon parameters used in these equations. These calculations predict that transient displacement of the crystal along the four B-symmetry phonons drives the system into a chiral state, which is determined by the linear superposition of these modes. The induced chirality can be quantified by calculating an electric toroidal monopole as the order parameter (*24*) or by following a recently introduced geometrical approach (*23*, *25*).

Dynamics of chirality and optical activity

The displacement causes two optical effects on a time-delayed probe pulse, optical activity, which relates to the wanted induced chirality, and induced birefringence due to the breaking

Downloaded from https://www.science.org at Stiftung Deutsches Elektronen-Synchrotron on January 23, 2025

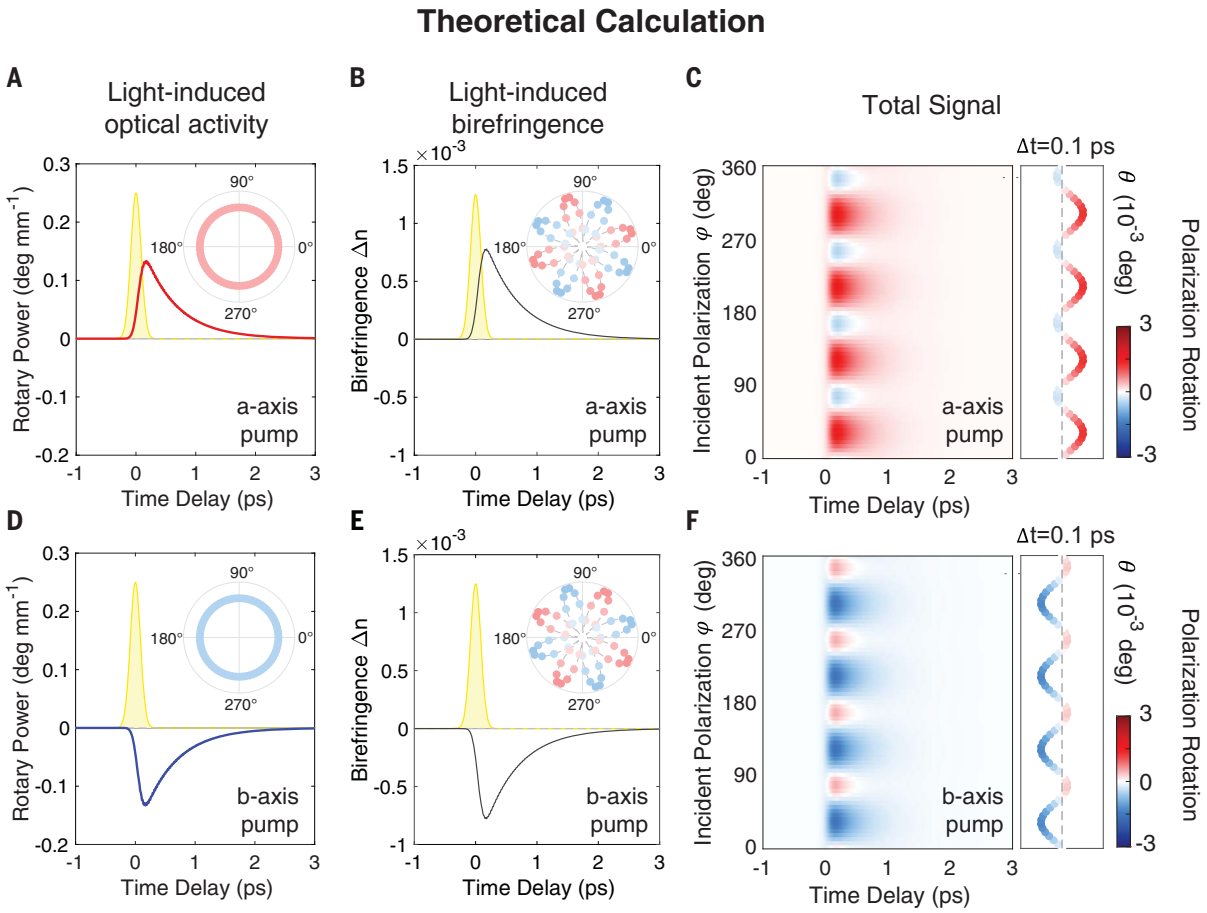

Fig. 3. Theoretical calculations of the light-induced chiral state. (**A**) Light-induced optical activity for the *a*-axis pump as a function of pump-probe time delay. The yellow-shaded area is the temporal profile of the excitation pulse. Inset shows the corresponding amplitude of the polarization rotation signal as a function of probe incident polarization. (**B**) Light-induced birefringence for the same *a*-axis pump as a function of pump-probe time delay. Inset shows the corresponding amplitude modulation of the polarization rotation signal as a function of probe incident polarization. (**C**) The resulting total polarization rotation signal for the *a*-axis pump as a function of probe incident polarization and pump-probe time delay. The signal at a fixed time delay of +0.1 ps is shown on the right. (**D**) Same as (A) but for excitation along the *b* axis. (**E**) Same as (B) but for excitation along the *b* axis. (**F**) Same as (C) but for excitation along the *b* axis. For all calculations, we used a 19-THz pump pulse of 5 MV/cm peak electric field.

of the fourfold symmetry (–4) of the crystal, which can be subtracted from the total optical signal to reveal the optical activity. Figure 3, A and B, shows the time-dependent changes of each of these properties (optical activity and induced birefringence) for excitation of the mode $Q_{E,a}$ along the *a* axis, as calculated from the transient lattice structure and taking into account the B-mode–dependent changes in the diagonal and off-diagonal elements of the optical permittivity. The latter were determined using an ab initio density functional theory approach (*23*).

The optical activity alone generates a characteristic polarization rotation that is independent of the incident polarization of the probe light in the *a*–*b* plane (*26*, *27*) (Fig. 3A, inset). Conversely, the birefringence introduces a modulation of the polarization rotation response with a fourfold symmetry with respect to the incident probe polarization [Fig. 3B, inset, and (*23*)] without changing the average value of the signal over all incident probe polarizations. The total polarization rotation signal follows the form

$$\theta(\varphi) = A_1\rho + A_2\sin(4\varphi - \phi)(\Delta n)^2 \qquad (3)$$

where φ is the relative angle between the pump and the probe polarization, ϕ is the angle between the pump polarization and the optical axis of the transient birefringence, ρ is the rotary power proportional to the optical activity, and Δn is the birefringence-induced difference in refractive index. The overall time-dependent polarization rotation signal, calculated as a function of the incident polarization, is shown for a terahertz pump with a peak electric field of 5 MV/cm (Fig. 3C).

When the polarization of the pump is oriented along the *b* axis to excite the mode $Q_{E,b}$, the induced displacement of the B-symmetry modes changes direction. Therefore, both the optical activity and the induced birefringence are reversed (Fig. 3, D and E), resulting in a sign change of the overall polarization rotation signal compared with the excitation along the *a* axis (Fig. 3F).

Experimental results

Experimental validation of these predictions was obtained using the optical setup sketched in Fig. 4A. The BPO_4 sample, held at room temperature, was excited by 19-THz center frequency pulses of 3 THz full width at half maximum, with an excitation fluence of up to 5.0 mJ/cm^2 and a corresponding peak electric field of 5.1 MV/cm. These pulses were linearly polarized along either the *a* or the *b* axis, resonantly driving each degenerate E-symmetry phonon mode at its 18.9-THz transverse-optical frequency (*23*).

A time-dependent rotation of the probe polarization was induced by phonon excitation with a pump polarized along the crystal *a* axis (Fig. 4B). At each probe polarization angle, we found a sudden onset of a rotation around

Downloaded from https://www.science.org at Stiftung Deutsches Elektronen-Synchrotron on January 23, 2025

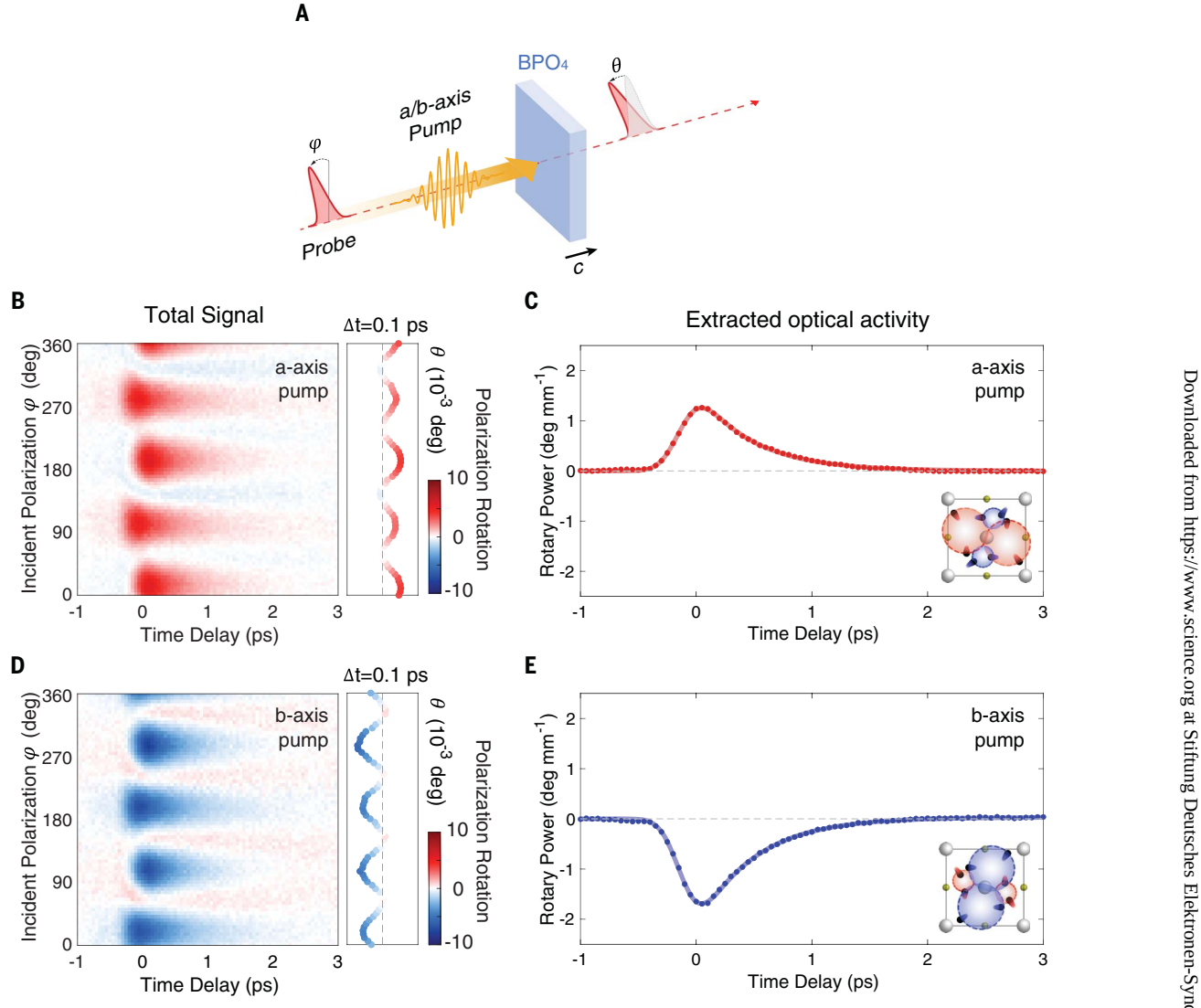

Fig. 4. Time-resolved polarization rotation measurements. (**A**) Schematic of the pump-probe experiment. A linearly polarized terahertz pulse, polarized along either the *a* or *b* axis, drives the BPO_4 crystal into chiral states. A time-delayed near-infrared pulse probes the state by the measurement of its polarization rotation, which is carried out as a function of the probe incident polarization. (**B**) Time delay–dependent polarization rotation signal for *a*-axis excitation as a function of probe incident polarization. The signal at a fixed time delay of +0.1 ps is shown on the right. (**C**) Time delay–dependent rotary power, proportional to the optical activity, extracted from the data shown in (B) and considering the finite extinction depth δ of the excitation pulses. (**D**) Same as (B) but for *b*-axis excitation. (**E**) Same as (C) but for *b*-axis excitation.

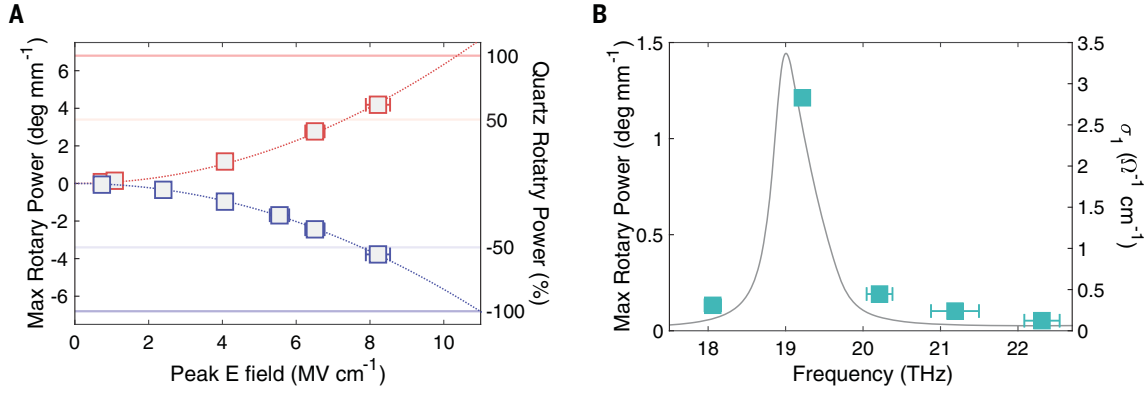

Fig. 5. Characterization of the light-induced chiral states. (**A**) The rotary power of the transient state as a function of the terahertz pulse peak electric field for a-axis–polarized (red) and b-axis–polarized (blue) excitation. (**B**) Maximum of rotary power at fixed peak electric field of 5.1 MV/cm as a function of the center frequency of the excitation pulse. The horizontal error bars are the 1σ confidence interval of the pump center frequency. Gray curve indicates the real part of the optical conductivity.

Downloaded from https://www.science.org at Stiftung Deutsches Elektronen-Synchrotron on January 23, 2025

time zero, followed by a decay lasting a few picoseconds, far longer than the 200-fs duration of the excitation pulse. The signal displayed a 90° periodicity with the incident probe polarization due to the transient birefringence discussed above.

Because of the modulation induced by the birefringence averaging to zero over all of the probe polarizations (*28*, *29*), the transient optical activity can be extracted by averaging the signal over all the incident probe polarizations at each time delay (Fig. 4C). The result shows a finite and positive signal, providing clear evidence for a nonequilibrium chiral state. Its lifetime follows the excitation and decay of the resonantly driven optical phonon.

We further rotated the pump polarization by 90° to resonantly drive the E-symmetry phonon along the BPO_4 crystal *b* axis. The corresponding time-dependent polarization rotation, again as a function of the incident probe polarization, and the corresponding optical activity are shown in Fig. 4, D and E. As predicted, the signals reversed sign, showing opposite handedness of the light-induced ferrichiral state compared with the *a*-axis excitation.

Further characterization of the light-induced chiral state validates the predicted nonlinear phononic mechanism. Figure 5A shows the rotary power as a function of the peak electric fields of the 19-THz excitation pulse, exhibiting a quadratic field dependence and a sign reversal for the two different pump polarizations. This behavior is consistent with the nonlinear phonon interaction potential $U = -\alpha Q_{E,a}^2 Q_B + \alpha Q_{E,b}^2 Q_B$. In addition, the magnitude of the nonequilibrium rotary power was resonantly enhanced when the excitation pulses were tuned to the 18.9-THz transverse optical frequency of the doubly degenerate E-symmetry phonon (Fig. 5B). We estimated the magnitude of the light-induced optical activity in BPO_4 at resonance by comparing the nonequilibrium rotary power with the static value of α-quartz (6.8°/mm), a commonly used material for polarization rotation in optics (*30*). For the pump fluence available in the experiment, and assuming that the chiral state is induced only within the extinction depth δ of the excitation pulses (*23*), the light-induced rotary power of BPO_4 is comparable to the equilibrium value of α-quartz.

Concluding remarks

Extension of this approach to ferrichiral systems may enable ultrafast switching with the nonlinear phononic protocol discussed here. Applications to ultrafast memory devices would follow, as well as to more sophisticated optoelectronic platforms powered by light and connected to the handedness of matter. More broadly, the emergence of chirality on the ultrafast time scale, together with the ability to switch between chirality of opposite handedness, offers exciting opportunities for exploring new phenomena in out-of-equilibrium physics of complex matter, especially in topological (*31*–*33*) and correlated systems (*34*, *35*), where handedness plays an important role.

REFERENCES AND NOTES

1. B. L. Feringa, R. A. Van Delden, *Angew. Chem. Int. Ed.* **38**, 3418–3438 (1999).
2. Y. Le Page, G. Donnay, *Acta Crystallogr. B* **32**, 2456–2459 (1976).
3. T. Matsuura, H. Koshima, *J. Photochem. Photobiol. Photochem. Rev.* **6**, 7–24 (2005).
4. N. Kumar, S. N. Guin, K. Manna, C. Shekhar, C. Felser, *Chem. Rev.* **121**, 2780–2815 (2021).
5. Y. Wang *et al*., *J. Am. Chem. Soc.* **145**, 17443–17460 (2023).
6. T. O. Yeates, S. B. Kent, *Annu. Rev. Biophys.* **41**, 41–61 (2012).
7. Z. Li *et al*., *Chem. Mater.* **16**, 2906–2908 (2004).
8. C. P. Romao, D. M. Juraschek, *ACS Nano* **18**, 29550–29557 (2024).
9. M. Först *et al*., *Nat. Phys.* **7**, 854–856 (2011).
10. P. G. Radaelli, *Phys. Rev. B* **97**, 085145 (2018).
11. X. Li *et al*., *Science* **364**, 1079–1082 (2019).
12. A. Stupakiewicz *et al*., *Nat. Phys.* **17**, 489–492 (2021).
13. A. S. Disa, T. F. Nova, A. Cavalleri, *Nat. Phys.* **17**, 1087–1092 (2021).
14. J. Luo *et al*., *Science* **382**, 698–702 (2023).
15. M. Fechner *et al*., *Nat. Mater.* **23**, 363–368 (2024).
16. M. Basini *et al*., *Nature* **628**, 534–539 (2024).
17. C. S. Davies *et al*., *Nature* **628**, 540–544 (2024).
18. D. Fausti *et al*., *Science* **331**, 189–191 (2011).
19. R. Mankowsky *et al*., *Nature* **516**, 71–73 (2014).
20. R. Mankowsky, A. von Hoegen, M. Först, A. Cavalleri, *Phys. Rev. Lett.* **118**, 197601 (2017).
21. T. F. Nova, A. S. Disa, M. Fechner, A. Cavalleri, *Science* **364**, 1075–1079 (2019).
22. A. S. Disa *et al*., *Nat. Phys.* **16**, 937–941 (2020).
23. Materials, methods, and additional information are available in the supplementary materials.
24. R. Oiwa, H. Kusunose, *Phys. Rev. Lett.* **129**, 116401 (2022).
25. G. H. Fecher, J. Kübler, C. Felser, *Materials* **15**, 5812 (2022).
26. F. Arago, *Sur une modification remarquable qu'éprouvent les rayons lumineux dans leur passage à travers certains corps diaphanes, et sur quelques autres nouveaux phénomènes d'optiques: Lu le 11 août 1811* (Firmin-Didot, 1812).
27. J.-B. Biot, *Mémoire sur un nouveau genre d'oscillation que les molécules de la lumiere éprouvent en traversant certains cristaux* (Chez Firmin Didot, 1814).
28. C. Rockstuhl, C. Menzel, T. Paul, F. Lederer, *Phys. Rev. B Condens. Matter Mater. Phys.* **79**, 035321 (2009).
29. M. Kuwata-Gonokami *et al*., *Phys. Rev. Lett.* **95**, 227401 (2005).
30. M. De Vido *et al*., *Opt. Mater. Express* **9**, 2708–2715 (2019).
31. A. Zyuzin, A. Burkov, *Phys. Rev. B Condens. Matter Mater. Phys.* **86**, 115133 (2012).
32. H. B. Nielsen, M. Ninomiya, *Phys. Lett. B* **130**, 389–396 (1983).
33. N. Ong, S. Liang, *Nat. Rev. Phys.* **3**, 394–404 (2021).
34. J. Ishioka *et al*., *Phys. Rev. Lett.* **105**, 176401 (2010).
35. S.-Y. Xu *et al*., *Nature* **578**, 545–549 (2020).

ACKNOWLEDGMENTS

We thank X. Deng and N. Taherian for help with the sample preparation and the optical setup, D. Nicoletti for help with the Fourier transform infrared characterization, X. Wang for help with the implementation of the optical activity calculations, P. Licht for technical assistance, and J. Harms for help with graphics. **Funding:** This work was supported by the Cluster of Excellence "CUI: Advanced Imaging of Matter" of the Deutsche Forschungsgemeinschaft (DFG) (EXC 2056, project ID 390715994). **Author contributions:** A.C. and Z.Z. conceived the project. Z.Z. and M.Fö. designed and performed the experiments with help from M.B. and E.B.A. P.D. grew the BPO_4 sample. C.P. and P.J.W.M. prepared the sample for the optical measurements. M.Fe. performed the DFT calculations and the simulations of the nonlinear phonon dynamics. Z.Z. analyzed the data with the help from M.Fö., M.Fe., M.B., and P.G.R. Z.Z., M.Fö., and A.C. wrote the manuscript with contributions from all other authors. **Competing interests:** The authors declare no competing interests. **Data and materials availability:** The data supporting the findings of this study are provided in the main text or the supplementary materials. **License information:** Copyright © 2025 the authors, some rights reserved; exclusive licensee American Association for the Advancement of Science. No claim to original US government works. https://www.science.org/about/science-licenses-journal-article-reuse

SUPPLEMENTARY MATERIALS

science.org/doi/10.1126/science.adr4713
Materials and Methods
Supplementary Text
Figs. S1 to S8
Tables S1 to S5
References (*36*–*48*)

Submitted 2 July 2024; accepted 22 November 2024
10.1126/science.adr4713

Downloaded from https://www.science.org at Stiftung Deutsches Elektronen-Synchrotron on January 23, 2025